Supplement S1

Expanded Background - Chlorophototrophy

Named for the chlorophyll and bacteriochlorophyll pigments that absorb light, chlorophototrophs drive both energy metabolism and redox chemistry via light. Found in cyanobacteria and at least seven other phototrophic clades of bacteria[1] it is responsible for the vast majority of primary production of biomass on Earth and much of the energy metabolism of organisms which possess it. Approximately 9,000 teramoles of carbon are fixed by chlorophototrophs annually[2], primarily via oxygenic photosynthesis and dwarfing other forms of primary production[3-5] (see Supplemental Figure 1).

The functional unit of the chlorophototrophic machinery is the photochemical reaction center, or RC. These large membrane-bound protein complexes are all descended from an ancestral homodimer[6], with some diversifying into heterodimers and some accumulating numerous accessory subunits[6, 7]. All chlorophototrophic reaction centers push electrons to reducing potentials via chlorophyll and bacteriochlorophyll photochemistry, either passing these electrons to electron carriers which can be used to fix biomass or energizing an electron transport chain to produce biologically available energy. Electrons may be sourced from metabolism via soluble cytochromes, or in the case of cyanobacterial Photosystem II, water itself. Chlorophyll and bacteriochlorophyll pigments are biochemically derived from porphyrins and evolutionarily related to heme, as indicated by the similarity of their biosynthesis[8-10]. Three central pairs of chlorophyll molecules in a transmembrane protein core represent the conserved engine of charge separation with one photo-excited chlorophyll donating an electron to another. Additional antenna chlorophylls in each reaction center allow absorption of light with a higher cross-section per

reaction center, with energy transferred from chlorophyll to chlorophyll via resonance transfer. The mass of the conserved core reaction center is approximately 150 kilodaltons[11] and when including these integrated antennas it can reach more than 350 kilodaltons[12]. Light-gathering capacity is further enhanced by the presence a remarkably diverse array of independently evolved pigment-bearing accessory antenna complexes[13, 14] which further transfer their absorbed energy into the reaction center.

Most commonly two protons are pumped per photon per photon absorbed, via a cytochrome bc proton-pumping complex (related to mitochondrial complex III) or an alternative complex III passing electrons between quinones and cytochromes. Up to four protons per photon is possible for some fraction of electrons in oxygenic phototrophs when a type I reaction center is used with electrons passing from ferredoxin through a complex I-like NDH complex and cytochrome b_6f [15-17].

Chlorophototrophy is found only in bacteria and in eukaryotes that have taken up photosynthetic cyanobacteria as plastid organelles, with no known archaeal chlorophototrophs. The distribution of chlorophototrophy within the bacteria is patchy[1] with chlorophototrophic clades scattered across the bacterial tree. Horizontal gene transfer is likely responsible for at least some of the distribution of chlorophototrophy across the tree of life with transfer positively identified into the Gemmatimonadetes, and within clades of the proteobacteria and chloroflexi[1, 18, 19]. However this process is rare at best with horizontal transfer requiring over 30 genes to move between species, and the relative importance of horizontal versus vertical transfer outside these examples is ambiguous[20]

The chlorophototrophic machinery has diversified significantly over time, with different lineages containing machinery that while operating from the same mechanistic basis has been adapted for different purposes. The deepest split in the evolutionary tree of reaction center proteins is that between type I and type II reaction centers (Figure 3, A and B). Type I reaction centers contain iron-sulfur clusters and are tuned to more reducing redox potentials, pushing electrons from cytochromes or other soluble electron carriers to ferredoxin (Figure 3A). Type II reaction centers are tuned to more oxidizing redox potentials, boosting electrons to membrane-soluble quinones from cytochromes (Figure 3B) or, in the case of cyanobacterial photosystem II, directly from water. While type I reaction centers produce a highly reduced electron carrier capable of driving either carbon fixation or energy metabolism, the quinone reduced by type II reaction centers cannot drive carbon fixation directly and instead can only directly drive an electron transport chain, typically consisting of a cytochrome bc complex[21, 22]

Extended Background - Retinalophototrophy

Retinalophototrophy, the second independent origin of phototrophy, was only discovered in the 1970s via investigation of the haloarchaea[23]. The retinalophototrophic system is far simpler than chlorophototrophy, consisting of a single 26-28 kilodalton transmembrane protein, known as a microbial or type-1 rhodopsin (in contrast to animal light sensor proteins, known as type-2 rhodopsins which have an uncertain relationship to these proteins). It is covalently bound to a single pigment molecule known as retinal, derived from the oxidative splitting of a carotenoid via a dioxygenase[24]. In a few cases, such as the xanthorhodopsins, a single additional carotenoid molecule is bound to the exterior of the protein and functions as a miniature integral ‘antenna’[25].

Microbial rhodopsins largely directly pump protons across a cell membrane rather than engaging in redox chemistry. Light-driven isomerization of the retinal pigment pumps a single proton per absorbed photon across the membrane through the rhodopsin channel[26], meaning the system is self-contained and does not require additional electron transport chain components to extract energy. Some rhodopsins, not directly involved in phototrophy, are also capable of pumping ions such as chloride or sodium and others function as light sensors[27]. There are no known autotrophs able to fix biomass from CO2 using only the energy derived from microbial rhodopsins (likely because the membrane voltage reached by microbial rhodopsins is insufficient to drive an electron transport chain in reverse for reverse electron flow). However, the energy generated by this system appears to be quite important for many photoheterotrophs. This energy can prevent starvation in marine bacteria[28], and is extensively used to supplement heterotrophic metabolism: the quantity of light absorbed by retinalophototrophs in the ocean is thought to be at least as large as that absorbed by chlorophototrophs[29].

The phylogenetic ubiquity of microbial rhodopsins, in contrast to the patchy distribution of chlorophototrophy, has only been fully appreciated in the last two decades. Approximately half of marine bacterial cells, from many taxa, bear diverse bacterial rhodopsin genes[30]. They are present in haloarchaea, marine bacteria[31], marine archaea[32], fungi[33], and heterotrophic marine eukaryotes[34] [35, 36]. They are known to acidify cellular compartments via pumping protons, and in some taxa are among the most highly expressed proteins[36], contributing significantly to the cell's energy budget. Poorly characterized rhodopsins which apparently pump protons inwards rather than outwards have even been discovered in metagenomes of Heimdallarchaea, a member of the Asgard archaea considered a likely sister to the archaeal

ancestor of eukaryotes[37, 38], and numerous marine viruses carry a variety of rhodopsin genes into their hosts[39, 40]}.

Microbial rhodopsins are exemplars of horizontal gene transfer, explaining its cosmopolitan distribution across the tree of life[41]. If a microbe contains a functional carotenoid synthesis pathway, retinalophototrophy may be transferred into the cell via a simple two-gene cassette consisting of the rhodopsin itself and a dioxygenase for retinal synthesis. If no carotenoid synthesis pathway exists, a total of five genes are required, constituting a basic carotenoid synthesis pathway alongside these genes[24, 42]. Gene cassettes of these types are widely observed in bacteria and archaea. Due to this extreme ease of horizontal gene transfer of rhodopsin systems compared to chlorophototrophic systems, the evolutionary origin of microbial rhodopsins remains unclear.

Despite this uncertainty, recent work has shed much light on their evolution and diversification[43, 44]. The deepest split in the tree of these proteins is the split between heliorhodopsins and all others. Heliorhodopsins share only small amounts of sequence homology with the rest of the rhodopsins, and are integrated into the cell membrane of organisms that bear them backwards, with the N terminus facing the interior face rather than the exterior as in all other rhodopsins[45]. Most heliorhodopsins have been found to not pump protons despite translocating protons between binding sites within themselves, have extremely slow photocycles, and often be fused with intracellular proteins[46], supporting a role as light sensors, although some with proton-pumping activity have been recently discovered[47]. In the set of non-heliorhodopsin microbial rhodopsins, the deepest split is between a large clade of poorly characterized viral rhodopsins and all others[44, 48]. Some of these viral rhodopsins are known to function as proton pumps in infected cells[40], while others seem to serve signaling functions altering the behavior of infected cells in response

to light. Within the remaining clade of rhodopsins found in cellular life, there is a significant diversity of proton pumping rhodopsins, sodium pumps, chloride pumps, light-activated passive channelrhodopsins, and sensory proteins spread between bacteria, archaea, and eukaryotes[44]. However, a recent work of ancestral sequence reconstruction on a subset of cellular microbial rhodopsins[49, 50] infers that the common ancestor of these cellular microbial rhodopsin was a proton pump capable of driving energy metabolism rather than a channel or pump for other ions or a sensory protein. It also infers an ancestral absorption peak at approximately 500 nanometers near the middle of the range of absorption peaks found in different rhodopsins. Together, the information on the phylogeny and diversification of rhodopsins supports placing the origins of retinalophototrophic energy metabolism at the very deepest branches of the rhodopsin phylogeny, if not even earlier.

Comparison of the Two Systems

The differences between chlorophototrophs and retinalophototrophs are manifold. Most trivially, the light-gathering pigments used by the core machinery of chlorophototrophs and retinalophototrophs are spectrally distinct. Retinal primarily absorbs the green wavelengths of visible light, while chlorophyll primarily absorbs in the red and blue wavelengths. This apparent partitioning of the electromagnetic spectrum is somewhat mitigated by the fact that chlorophototrophs contain many accessory pigments aside from basic chlorophyll which can expand their effective absorption spectrum into the green wavelengths.

One of the greatest physiological differences between retinalophototrophs and chlorophototrophs is the maximum efficiency of conversion of light energy into biologically available energy. Chlorophototrophs have a significantly higher energy yield per captured photon than

retinalophototrophs. Retinalophototrophic machinery pumps one proton per photon across the cell membrane, while the chlorophototrophic machinery is capable of pumping multiple protons per photon. Most commonly two protons are pumped per photon, via a cytochrome bc proton-pumping complex (related to mitochondrial complex III) or an alternative complex III passing electrons between quinones and cytochromes. Up to four protons per photon are possible for some fraction of electrons in oxygenic phototrophs when a type I reaction center is used with electrons passing from ferredoxin through a complex I-like NDH complex and cytochrome b_6f[15-17]. However the difference in available energy may be even greater than this ratio would indicate, as microbial rhodopsins are incapable of pumping against a membrane polarization of ~200 mV[51] which is lower than the proton motive force generated by respiratory electron transport chains. The electron transport chains of chlorophototrophs are thus able to conserve more energy per proton than rhodopsins are by reaching a higher membrane voltage. Furthermore, electrons energized by some chlorophototrophic reaction centers may be passed to electron carriers such as ferredoxin and NADPH, or the high proton-motive force they generate can be used to force reverse electron flow through a respiratory electron transport chain into these carriers for carbon and nitrogen fixation. Retinalophototrophs are unable to produce biomass *de novo* using their phototrophic machinery, likely due to their low maximum proton-motive force being insufficient to allow reverse electron flow.

The material composition of the phototrophic machinery in retinalophototrophs and chlorophototrophs is also quite different. While microbial rhodopsins consist of a single ~27 kDa protein molecule attached to one or at most two photoactive cofactors per functional unit, chlorophototrophic reaction centers consist of 2-4 core protein molecules and a number of accessory proteins per functional unit with a mass of up to 350 kDa[7], with a large number of

diverse photopigments bound to each complex. Moreover, nearly every chlorophototrophic reaction center is associated with multiple diverse antenna complexes, which both greatly increases the absorption cross section per functional unit and can bring the total protein mass per functional unit into the megadaltons or even more[13, 52]. This increased absorption cross section leads to a significantly greater efficiency in terms of captured biological energy per unit incident light at low light intensities for chlorophototrophs, at the expense of saturation at relatively low light levels.

Another physiologically and ecologically important difference between chlorophototrophs and retinalophototrophs is the requirement for iron in the chlorophototrophic machinery. While bacterial rhodopsins are entirely composed of protein and organic molecules, every known chlorophototrophic reaction center contains iron atoms. All type I reaction centers contain at least 4 in an Fe-S cluster in the core dimer, with 12 known when including accessory subunits in the case of acidobacteria, chlorobi, and photosystem I of cyanobacteria[12, 53, 54] and some may be complexed with additional integrated cytochromes bearing heme irons[55]. All type II reaction centers contain one Fe^{2+} ion bound at the interface between subunits with additional heme irons present in Photosystem II of cyanobacteria[7] and an integral cytochrome with additional heme irons present in the reaction centers of many other lineages[56-58]. All known electron transport chains that chlorophototrophic reaction centers participate in also utilize iron in their proton-pumping components, with 6 iron atoms present in each subunit of cyanobacterial cytochrome b_6f[59] and the NDH complex used for circular electron flow around Photosystem I containing at least twelve or possibly more[16, 17]. Certain picocyanobacteria reduce their electron transport chains to a form which requires nearly only the iron atoms in the photosystems themselves (biased towards photosystem II with fewer iron atoms) and an alternative oxidase, but this comes at the expense of depressing proton pump yield to only one proton per photon[60].

This constitutive requirement of iron for functional chlorophototrophy but not retinalophototrophy represents a major resource limitation for chlorophototrophs, especially in oligotrophic environments such as the open ocean where iron levels are limiting[61]. This represents a trade-off between the two systems, with the enhanced yield per unit light of retinalophototrophy and the ability to perform redox reactions dependent upon use of a limiting mineral nutrient. This trade-off is apparent in marine diatoms, one of a few known groups[33, 62] to bear both rhodopsins and chlorophototrophic reaction centers[63]. These organisms significantly upregulate rhodopsin expression upon iron starvation[63, 64]. This trade-off thus appears to be physiologically relevant, at least in areas of iron limitation.

Works Cited:

1. Thiel, V., M. Tank, and D.A. Bryant, *Diversity of Chlorophototrophic Bacteria Revealed in the Omics Era.* Annu Rev Plant Biol, 2018. **69**: p. 21-49.
2. Field, C.B., et al., *Primary production of the biosphere: integrating terrestrial and oceanic components.* science, 1998. **281**(5374): p. 237-240.
3. Raven, J.A., *Contributions of anoxygenic and oxygenic phototrophy and chemolithotrophy to carbon and oxygen fluxes in aquatic environments.* Aquatic Microbial Ecology, 2009. **56**(2-3): p. 177-192.
4. Sleep, N.H. and D.K. Bird, *Niches of the pre-photosynthetic biosphere and geologic preservation of Earth's earliest ecology.* Geobiology, 2007. **5**(2): p. 101-117.
5. Canfield, D.E., M.T. Rosing, and C. Bjerrum, *Early anaerobic metabolisms.* Philosophical Transactions of the Royal Society B: Biological Sciences, 2006. **361**(1474): p. 1819-1836.
6. Cardona, T., *A fresh look at the evolution and diversification of photochemical reaction centers.* Photosynth Res, 2015. **126**(1): p. 111-34.
7. Umena, Y., et al., *Crystal structure of oxygen-evolving photosystem II at a resolution of 1.9 Å.* Nature, 2011. **473**(7345): p. 55-60.
8. Chew, A.G. and D.A. Bryant, *Chlorophyll biosynthesis in bacteria: the origins of structural and functional diversity.* Annu Rev Microbiol, 2007. **61**: p. 113-29.
9. Martin, W.F., D.A. Bryant, and J.T. Beatty, *A physiological perspective on the origin and evolution of photosynthesis.* FEMS Microbiol Rev, 2018. **42**(2): p. 205-231.
10. Bryant, D.A., C.N. Hunter, and M.J. Warren, *Biosynthesis of the modified tetrapyrroles-the pigments of life.* J Biol Chem, 2020. **295**(20): p. 6888-6925.
11. Niwa, S., et al., *Structure of the LH1–RC complex from Thermochromatium tepidum at 3.0 Å.* Nature, 2014. **508**(7495): p. 228-232.
12. Fromme, P., P. Jordan, and N. Krauß, *Structure of photosystem I.* Biochimica et Biophysica Acta (BBA)-Bioenergetics, 2001. **1507**(1-3): p. 5-31.
13. Bryant, D.A. and D.P. Canniffe, *How nature designs light-harvesting antenna systems: design principles and functional realization in chlorophototrophic prokaryotes.* Journal of Physics B: Atomic, Molecular and Optical Physics, 2018. **51**(3): p. 033001.
14. Kouyianou, K., et al., *The chlorosome of Chlorobaculum tepidum: size, mass and protein composition revealed by electron microscopy, dynamic light scattering and mass spectrometry-driven proteomics.* Proteomics, 2011. **11**(14): p. 2867-80.
15. Nawrocki, W., et al., *The mechanism of cyclic electron flow.* Biochimica et Biophysica Acta (BBA)-Bioenergetics, 2019.
16. Zhu, J., K.R. Vinothkumar, and J. Hirst, *Structure of mammalian respiratory complex I.* Nature, 2016. **536**(7616): p. 354-358.
17. Shikanai, T., *Chloroplast NDH: A different enzyme with a structure similar to that of respiratory NADH dehydrogenase.* Biochim Biophys Acta, 2016. **1857**(7): p. 1015-22.
18. Brinkmann, H., et al., *Horizontal operon transfer, plasmids, and the evolution of photosynthesis in Rhodobacteraceae.* ISME J, 2018. **12**(8): p. 1994-2010.
19. Zeng, Y., et al., *Functional type 2 photosynthetic reaction centers found in the rare bacterial phylum Gemmatimonadetes.* Proc Natl Acad Sci U S A, 2014. **111**(21): p. 7795-800.

20. Cardona, T., *Thinking twice about the evolution of photosynthesis.* Open Biol, 2019. **9**(3): p. 180246.
21. Schutz, M., et al., *Early evolution of cytochrome bc complexes.* J Mol Biol, 2000. **300**(4): p. 663-75.
22. Hohmann-Marriott, M.F. and R.E. Blankenship, *Evolution of photosynthesis.* Annu Rev Plant Biol, 2011. **62**: p. 515-48.
23. Oesterhelt, D. and W. Stoeckenius, *Rhodopsin-like Protein from the Purple Membrane of Halobacterium halobium.* Nature New Biology, 1971. **233**(39): p. 149-152.
24. Sabehi, G., et al., *New insights into metabolic properties of marine bacteria encoding proteorhodopsins.* PLoS Biol, 2005. **3**(8): p. e273.
25. Balashov, S.P., et al., *Xanthorhodopsin: a proton pump with a light-harvesting carotenoid antenna.* Science, 2005. **309**(5743): p. 2061-4.
26. Ernst, O.P., et al., *Microbial and animal rhodopsins: structures, functions, and molecular mechanisms.* Chem Rev, 2014. **114**(1): p. 126-63.
27. Govorunova, E.G., et al., *Microbial Rhodopsins: Diversity, Mechanisms, and Optogenetic Applications.* Annu Rev Biochem, 2017. **86**: p. 845-872.
28. Gómez-Consarnau, L., et al., *Proteorhodopsin Phototrophy Promotes Survival of Marine Bacteria during Starvation.* PLOS Biology, 2010. **8**(4): p. e1000358.
29. Gómez-Consarnau, L., et al., *Microbial rhodopsins are major contributors to the solar energy captured in the sea.* Science advances, 2019. **5**(8): p. eaaw8855.
30. Finkel, O.M., O. Béjà, and S. Belkin, *Global abundance of microbial rhodopsins.* The ISME Journal, 2013. **7**(2): p. 448-451.
31. Béja, O., et al., *Bacterial rhodopsin: evidence for a new type of phototrophy in the sea.* Science, 2000. **289**(5486): p. 1902-1906.
32. Rinke, C., et al., *A phylogenomic and ecological analysis of the globally abundant Marine Group II archaea (Ca. Poseidoniales ord. nov.).* The ISME Journal, 2019. **13**(3): p. 663-675.
33. Gleason, F.H., et al., *Ecological implications of recently discovered and poorly studied sources of energy for the growth of true fungi especially in extreme environments.* Fungal ecology, 2019. **39**: p. 380-387.
34. Slamovits, C.H., et al., *A bacterial proteorhodopsin proton pump in marine eukaryotes.* Nature Communications, 2011. **2**(1): p. 183.
35. Vader, A., et al., *Proton-pumping rhodopsins are abundantly expressed by microbial eukaryotes in a high-Arctic fjord.* Environmental Microbiology, 2018. **20**(2): p. 890-902.
36. Labarre, A., et al., *Expression of genes involved in phagocytosis in uncultured heterotrophic flagellates.* Limnology and Oceanography, 2020. **65**(S1): p. S149-S160.
37. Bulzu, P.-A., et al., *Casting light on Asgardarchaeota metabolism in a sunlit microoxic niche.* Nature microbiology, 2019. **4**(7): p. 1129-1137.
38. Inoue, K., et al., *Schizorhodopsins: A family of rhodopsins from Asgard archaea that function as light-driven inward H⁺ pumps.* Science Advances, 2020. **6**(15): p. eaaz2441.
39. Yutin, N. and E.V. Koonin, *Proteorhodopsin genes in giant viruses.* Biology direct, 2012. **7**(1): p. 1-6.
40. Needham, D.M., et al., *A distinct lineage of giant viruses brings a rhodopsin photosystem to unicellular marine predators.* Proceedings of the National Academy of Sciences, 2019. **116**(41): p. 20574-20583.

41. Sharma, A.K., J.L. Spudich, and W.F. Doolittle, *Microbial rhodopsins: functional versatility and genetic mobility.* Trends in microbiology, 2006. **14**(11): p. 463-469.
42. Pinhassi, J., et al., *Marine bacterial and archaeal ion-pumping rhodopsins: genetic diversity, physiology, and ecology.* Microbiology and Molecular Biology Reviews, 2016. **80**(4): p. 929-954.
43. Nagata, T. and K. Inoue, *Rhodopsins at a glance.* Journal of Cell Science, 2021. **134**(22): p. jcs258989.
44. Rozenberg, A., et al., *Microbial Rhodopsins: The Last Two Decades.* Annual Review of Microbiology, 2021. **75**: p. 427-447.
45. Pushkarev, A., et al., *A distinct abundant group of microbial rhodopsins discovered using functional metagenomics.* Nature, 2018. **558**(7711): p. 595-599.
46. Bulzu, P.-A., et al., *Heliorhodopsin Evolution Is Driven by Photosensory Promiscuity in Monoderms.* mSphere, 2021. **6**(6): p. e0066121.
47. Hososhima, S., et al., *Proton-transporting heliorhodopsins from marine giant viruses.* bioRxiv, 2022.
48. Philosof, A. and O. Béjà, *Bacterial, archaeal and viral-like rhodopsins from the R ed S ea.* Environmental microbiology reports, 2013. **5**(3): p. 475-482.
49. Sephus, C.D., et al., *Functional divergence and spectral tuning of microbial rhodopsins from an ancestral proton pump.* bioRxiv, 2021.
50. Sephus, C.D., et al., *Earliest photic zone niches probed by ancestral microbial rhodopsins.* Molecular Biology and Evolution, 2022. **39**(5): p. msac100.
51. Walter, J.M., et al., *Light-powering Escherichia coli with proteorhodopsin.* Proceedings of the National Academy of Sciences, 2007. **104**(7): p. 2408-2412.
52. Zhang, J., et al., *Structure of phycobilisome from the red alga Griffithsia pacifica.* Nature, 2017. **551**(7678): p. 57-63.
53. He, G., et al., *Structural analysis of the homodimeric reaction center complex from the photosynthetic green sulfur bacterium Chlorobaculum tepidum.* Biochemistry, 2014. **53**(30): p. 4924-4930.
54. Tsukatani, Y., et al., *Isolation and characterization of homodimeric type-I reaction center complex from Candidatus Chloracidobacterium thermophilum, an aerobic chlorophototroph.* Journal of Biological Chemistry, 2012. **287**(8): p. 5720-5732.
55. He, Z., et al., *Reaction centers of the thermophilic microaerophile, Chloracidobacterium thermophilum (Acidobacteria) I: biochemical and biophysical characterization.* Photosynthesis research, 2019. **142**(1): p. 87-103.
56. Nagashima, S. and K.V. Nagashima, *Comparison of photosynthesis gene clusters retrieved from total genome sequences of purple bacteria,* in *Advances in Botanical Research*. 2013, Elsevier. p. 151-178.
57. Xin, Y., et al., *Cryo-EM structure of the RC-LH core complex from an early branching photosynthetic prokaryote.* Nature communications, 2018. **9**(1): p. 1-10.
58. Ward, L.M., T. Cardona, and H. Holland-Moritz, *Evolutionary Implications of Anoxygenic Phototrophy in the Bacterial Phylum Candidatus Eremiobacterota (WPS-2).* Front Microbiol, 2019. **10**: p. 1658.
59. Kurisu, G., et al., *Structure of the cytochrome b6f complex of oxygenic photosynthesis: tuning the cavity.* Science, 2003. **302**(5647): p. 1009-1014.

60. Braakman, R., M.J. Follows, and S.W. Chisholm, *Metabolic evolution and the self-organization of ecosystems.* Proceedings of the National Academy of Sciences, 2017. **114**(15): p. E3091-E3100.
61. Sieradzki, E.T., et al., *Proteorhodopsins dominate the expression of phototrophic mechanisms in seasonal and dynamic marine picoplankton communities.* PeerJ, 2018. **6**: p. e5798.
62. Choi, A.R., et al., *Cyanobacterial light-driven proton pump, Gloeobacter rhodopsin: complementarity between rhodopsin-based energy production and photosynthesis.* PloS one, 2014. **9**(10): p. e110643.
63. Marchetti, A., et al., *Comparative metatranscriptomics identifies molecular bases for the physiological responses of phytoplankton to varying iron availability.* Proceedings of the National Academy of Sciences, 2012. **109**(6): p. E317-E325.
64. Marchetti, A., et al., *Marine diatom proteorhodopsins and their potential role in coping with low iron availability.* The ISME Journal, 2015. **9**(12): p. 2745-2748.

Supplement S2

Calculation of phototrophic energy fluxes per unit mass at different light levels for modern phototrophic systems

The 'return on investment' of a modern phototrophic system is taken in this work to be the energy flux per unit mass of the dedicated phototrophic machinery at a given light level. Recycling rate of individual proteins within individual modern phototrophic machineries was beyond the scope of this review to incorporate due to the widely varying half-life or dilution rates of different components under different environments, and as such energy fluxes are measured in energy flux per unit mass rather than energy yield per unit of protein synthesis.

To calculate the maximum mass-specific energetic rate of return (V_{max}) on investment of retinalophototrophic versus chlorophototrophic systems, the total mass per functional phototrophic unit (M_{total}), the cycling rate (R_{max}), and the protons pumped per cycle (N_p) must be known. V_{max} is equal to the product of N_p and R_{max} divided by M_{total}, as described in the following equation:

Equation S1: $V_{max} = N_p \cdot R_{max}/M_{total}$

Two retinalophototrophic systems, bacteriorhodopsin and proteorhodopsin, and two chlorophototrophic systems, oxygenic photosynthesizers and purple bacteria, were considered for breadth. Bacteriorhodopsin is described as a functionally monomeric 26 kDa protein [1]and proteorhodopsin is described as a functionally monomeric 27 kDa protein [2].

In the case of complex chlorophototrophic systems, the total mass per functional phototrophic unit must be calculated to include the mass of any antenna complexes associated with a chlorophototrophic reaction center. This was done by multiplying the mass of each antenna complex by the number of antenna complexes per photosynthetic unit at their in vivo stoichiometry, and adding this to the total mass of the active center. There are few cases in which every reaction center and antenna complex in a single organism are structurally understood and the stoichiometry of each component is known. Thus, in order to estimate the total mass of a functional unit of chlorophototrophic machinery it is necessary to use data from multiple functionally similar organisms to infer an approximate value.

An oxygenic chlorophototrophic reaction center was taken to be a single instance of either photosystem I (PSI) or photosystem II (PSII). As described in Cunningham et al., 1989 [3], the ratio of PSII : PSI : Phycobilisome in the oxygenic red algae *Porphyridium cruentum* (ATCC 50161) in low light (6 μmol photons m^{-2} s^{-1}) is 2.85 : 5.35 : 1 and in high light (280 μmol photons m^{-2} s^{-1}) the ratio is 3.96 : 7.59 : 1. The average across all conditions tested was 3.13 PSII : 6.50 PSI : 1 phycobilisome in this red algae. The mass of PSII is taken to be 350 kDa as described for *Thermosynechococcus vulcanis* in Umena et al., 2011 [4], the mass of PSI is taken to be 356 kDa as described for *Synechococcus elongates* in Fromme et al., 2001 [5], and the mass of a phycobilisome antenna complex is taken to be 16.2 mDa as described for the red algae *Griffithsia pacifica* in Zhang et al., 2017 [6]. This brings the total mass of an approximated stoichiometric unit with 9.63 reaction centers (RCs) and one phycobilisome to approximately 20.2 mDa and the total mass per reaction center to 2098 kDa.

The mass of antenna complexes other than phycobilisomes in oxygenic chlorophototrophs was not considered due to diversity in antenna complexes present in different organisms. The mass of other electron transport chain components or membrane ATPases was not considered due to likely low but poorly constrained stoichiometries [7], low masses compared to phycobilisomes [8], and their use in multiple cellular processes compared to the comparatively dedicated chlorophototrophic machinery.

Table S1: Mass estimation per oxygenic chlorophototrophic reaction center

Component	Number per stoichiometric unit	Mass
PSII	3.13	350 kDa
PSI	6.50	356 kDa
Phycobilisome	1	16.2 mDa
Total (9.63 RC plus phycobilisome)		20.2 mDa
Mass per RC (M_{total})		2098 kDa

A representative anoxygenic chlorophototrophic system from the purple bacteria species *Rhodospirillum photometricum* was examined for comparison, as described by Scheuring & Sturgis, 2009 [9]. In this species, each type-II reaction center is associated with one complex of 16 LH1 antenna proteins, forming a ‘core complex’, and multiple rings of 9 LH2 antenna proteins. The core complex:LH2 complex ratio was taken to be 3.5, as observed at high light adaptation in this work. The mass of the RCII/LH1 core complex described in Niwa et al., 2014 [10] in the purple bacterium *Thermochromatium tepidum* is 380 kDa. The measured mass of the

LH2 complex described by Cherezov et al., 2006 [11] in the purple bacterium *Rps acidophila* is 130 kDa. This brings the total mass of a stoichiometric unit containing a single RC to approximately 835 kDa. Again, the mass of additional electron transport chain components was not considered due to the multiple roles of these components in other cellular processes and low apparent stoichiometry relative to other chlorophototrophic machinery [7].

Table S2: Mass estimation per anoxygenic purple bacteria chlorophototrophic reaction center

Component	Number per stoichiometric unit	Mass
RC + LH1	1	380 kDa
LH2	3.5	130 kDa
Mass per RC (M_{total})		835 kDa

Field measurements of the maximum cycling rate of chlorophototrophic reaction centers from Kolber et al., 2000 [12] were used along with these figures to estimate the maximum energy flux per unit protein available to chlorophototrophs. In saturating light levels, oxygenic phototrophic phytoplankton were measured to have a maximum sustainable rate of reaction center photocycling of approximately 350 per second, and aerobic anoxygenic phototrophs were measured to reach up to approximately 150 per second. These are broadly consistent with in vitro measurements of photosystem II photocycle rate of more than 200 cycles per second observed in isolated photosystems by Lubner et al., 2011 [13]. Each photocycle of a reaction center was taken to represent two protons pumped across the photosynthetic membrane by the cytochrome b_6f complex in oxygenic chlorophototrophs or other electron transport chain components in anoxygenic chlorophototrophs. Electron transport chains containing the Complex-I like NDH

complex (likely capable of pumping additional protons) rather than cytochrome b_6f alone was not considered due to a low apparent rate of cycling and low stoichiometry, suggesting that while necessary for regulatory purposes it is not a primary player in energy metabolism [14].

Microbial rhodopsins were represented by proteorhodopsin which has been measured at being capable of 25 pumping protons per second in Friedrich et al., 2002 [15] and bacteriorhodopsin measured at approximately 50-100 protons per second in Béja et al., 2000 [2] and Lanyi, 2006 [16]. We took the bacteriorhodopsin maximum cycling rate to be 100 protons per second. In all cases, energy flux was calculated as described in equation S1.

Table S3: Maximum energy flux per unit mass for chlorophototrophy and retinalophototrophy

	Proteorhodopsin	Bacteriorhodopsin	Oxygenic RC	Anoxygenic RC
M_{total} (kDa)	27	26	2098	835
R_{max} (cycles s^{-1})	25	100	350	150
N_p (protons $cycle^{-1}$)	1	1	2	2
$R_{max} \cdot N_p$ (Protons s^{-1})	25	100	700	300
V_{max} (Protons kDa^{-1} s^{-1})	0.93	3.85	0.33	0.36

The response of the energy flux per kilodalton of protein mass (F_P) in chlorophototrophs and retinalophototrophs to varying light levels (L) was modeled via simple Michaelis–Menten kinetics, using the following equation:

Equation S2: $\boldsymbol{F_P = \frac{V_{max} \cdot L}{K_m + L}}$

V_{max} was taken to be the previously calculated maximum energy flux rate of a phototrophic system in protons kDa^{-1} s^{-1}. K_m represents the light level at which the energy flux per functional unit reaches its half-maximum. The K_m for both proteorhodopsin and bacteriorhodopsin was taken to be 2700 μmol m^{-2} s^{-1}, as described for proteorhodopsin in Walter et al., 2007 [17]. The K_m for oxygenic RCs was taken to be 40 μmol m^{-2} s^{-1} and the K_m for an anoxygenic RC was taken to be 191 μmol m^{-2} s^{-1}, as described in Kirchman and Hanson, 2013 [18].

Table S4: K_m, V_{max} for energy flux per unit mass for chlorophototrophy and retinalophototrophy

	Proteorhodopsin	Bacteriorhodopsin	Oxygenic RC	Anoxygenic RC
K_m (μmol m^{-2} s^{-1})	2700	2700	40	191
V_{max} (Protons kDa^{-1} s^{-1})	0.93	3.85	0.33	0.36

The relationship between light intensity and the energy flux per unit protein per unit incident light for each phototrophic system was calculated using equation S3, derived by dividing Equation S2 by light intensity, yielding the following equation.

Equation S3: $F_L = \frac{V_{max}}{K_m + L}$

The flux F_L, in units of protons kDa^{-1} s^{-1} / (μmol m^{-2} s^{-1}), represents the specific energy flux of a unit of protein machinery per unit incident light, and is reduced upon saturation of the machinery with light. It is thus maximized at low light. The form that this efficiency curve takes is similar to that determined from first-principles modeling of anoxygenic chlorophototrophic machinery in Sener et al., 2019 [19].

The maximum yield per unit incident light was calculated by setting [light intensity] equal to zero, at which point the value of Equation S3 is maximized and the largest marginal return per unit incident light is achieved. This value is represented by the following equation:

Equation S4: $Y_{max} = V_{max}/K_m$

This maximum yield represents the highest efficiency available per available light resource, reached at infinitesimal light levels.

Table S5: Maximum yield Y_{max} for chlorophototrophy and retinalophototrophy

	Proteorhodopsin	Bacteriorhodopsin	Oxygenic RC	Anoxygenic RC
Y_{max} (protons kDa^{-1} s^{-1} / (μmol m^{-2} s^{-1}))	$3.43 \cdot 10^{-4}$	$1.43 \cdot 10^{-3}$	$8.34 \cdot 10^{-3}$	$1.88 \cdot 10^{-3}$

It is important to note that a large fraction of the difference in efficiency per unit incident light between chlorophototrophic and retinalophototrophic machinery is due not to the greater quantum yield of chlorophototrophic machinery per unit absorbed photon, but instead is simply due to a much larger absorption cross section per functional unit due to a much larger amount of dedicated light-gathering protein machinery per unit. However, the total absorption cross section per unit infrastructure for chlorophototrophs and retinalophototrophs is quite similar.

The protein infrastructure mass per unit absorption ($\underline{M_{cs}}$) of a phototrophic system measures how efficiently light is captured. It is calculated from the mass per functional unit (M_{total}) and the absorption cross section per functional unit (Cs). The cross-section per functional unit is taken

from Kirchman and Hanson, 2013 [18], in which it is approximated for all rhodopsins (2 $Å^2$), an oxygenic phototroph (100 $Å^2$), and an anoxygenic phototroph (50 $Å^2$) based on a compilation of experiments and the light spectrum available in a marine environment. This is represented by the following equation:

Equation S5: $M_{cs} = M_{total}/Cs$

The mass per unit light-absorbing cross section is measured in in units of kDa $Å^{-2}$.

While a large amount of the difference in efficiency per unit incident light is explicable in terms of the difference in total mass per functional unit, the enhanced quantum yield of chlorophototrophic machinery in terms of protons pumped per photon absorbed is an important difference between the two forms of phototrophy. Thus, to account for the greater yield per absorbed photon, the mass per unit cross section is normalized using the following equation:

Equation S6: $NormalizedM_{cs} = M_{cs}/Yield$

This normalized mass per unit cross section accounts for the fact that photons absorbed by chlorophototrophic machinery are used to energize an electron transport chain and are capable of pumping ~2 protons per photon rather than the 1 proton per photon of retinalophototrophic machinery, and are thus twice as efficient in terms of yield per unit incident light.

Table S6: mass per unit cross section calculation for chlorophototrophy and retinalophototrophy

	Proteorhodopsin	Bacteriorhodopsin	Oxygenic RC	Anoxygenic RC
M_{total} (kDa)	27	26	2098	835

Cs ($Å^2$)	2	2	100	50
M_{cs} (kDa $Å^{-2}$)	13.5	13	20.98	16.7
Yield (protons/photon)	1	1	2	2
Yield-Normalized M_{cs} (kDa $Å^{-2}$)	13.5	13	10.49	8.35

Mathematical analysis of tradeoffs between efficiency per unit resource and efficiency per unit protein machinery

In order to mathematically examine the tradeoff between efficiency per unit incident light, and efficiency per unit protein infrastructure, the structure of phototrophic machinery was simplified into an eight-parameter model using Matlab. All phototrophic systems were conceptualized as an invariant catalytic core coupled to a variable quantity of 'antenna' machinery. Antenna increases absorption cross section while not being catalytically active. The catalytic core transduces light energy into biologically available energy (high potential electrons used to run an electron transport chain in the case of chlorophototrophic machinery, and directly pumped protons in the case of retinalophototrophic machinery). Both components are subject to photodegradation.

The antenna mass will be denoted by the variable *x*, in units of kilodaltons. As the total antenna mass per catalytic core will be allowed to vary, the absorption cross section of the antenna will be denoted by the variable a in units of square angstroms per kilodalton.

The catalytic core mass will be denoted by the variable *k*, in units of kilodaltons. Its intrinsic absorption cross section will be denoted by the variable *b*, in units of square angstroms. Its maximum rate of turnover will be denoted by the variable *Vmax*, in terms of cycles per second. Its yield will be denoted by the variable *Y*, in terms of protons pumped per photocycle.

Michaelis-Menten kinetics were used to model the operation of the phototrophic machinery. As such, the K_m of the system (Equation S7) was taken to be the maximum reaction rate of the central engine over the total absorption cross section of the system:

Equation S7: $K_m = \frac{V_{max}}{ax+b}$

The energy flux per unit phototrophic machinery *F* (protons pumped per second) at a given light intensity is denoted by Equation S8, multiplying the standard Michaelis-Menten reaction rate (using light intensity *L* as substrate availability) by the yield per photocycle:

Equation S8: $F = Y \cdot \frac{V_{max} \cdot L}{K_m + L} = \frac{Y \cdot L \cdot V_{max}}{\left(\frac{Vmax}{ax+b}\right) + L} = \frac{Y \cdot L \cdot V_{max} \cdot (ax+b)}{V_{max} + L \cdot (ax+b)}$

The energy flux per unit protein F_p (protons pumped per kilodalton per second) is denoted by Equation S9, dividing *F* by the total mass of the phototrophic machinery:

Equation S9: $F_P = \frac{F}{k+x} = Y \cdot \frac{V_{max} \cdot L}{K_m + L} * \frac{1}{k+x} = \frac{Y \cdot L \cdot V_{max} \cdot (ax+b)}{(k+x) \cdot (V_{max} + L \cdot (ax+b))}$

The energy flux per unit incident light (protons pumped per kilodalton per second per unit photons per square angstrom per second) is denoted by equation S10, dividing F_p by *L*:

Equation S10: $F_L = Y \cdot \frac{V_{max} \cdot L}{K_m + L} \cdot \frac{1}{k+x} \cdot \frac{1}{L} = \frac{Y \cdot V_{max} \cdot (ax+b)}{(k+x) \cdot (V_{max} + L \cdot (ax+b))}$

Equations S8 through S10 describe the throughput of phototrophic machinery that is fully functional, but light degrades the machinery via photodegradation. To take this into account, methods of Han, 2002[20] and Faizi et al., 2018[21] were used in which photodegradation is proportional to the rate of photon absorption by excited phototrophic machinery. This follows equation S11, in which the rate of photodegradation v_i in fractions of total protein per second is dependent on the photodegradation rate constant D (in units of photon^{-1}), absorption cross section ($ax+b$) in square angstroms, light intensity L in photons per square angstrom per second, and fraction of the phototrophic machinery excited P^*.

Equation S11: $v_i = D \cdot (ax + b) \cdot L \cdot P^*$

Using a two-state model, the fraction of phototrophic machinery excited is taken to be equal to the ratio of the current reaction rate to the V_{max} resulting in equation S12:

Equation S12: $v_i = D \cdot (ax + b) \cdot L \cdot \frac{L \cdot V_{max} \cdot (ax+b)}{V_{max} + L \cdot (ax+b)} \cdot \frac{1}{V_{max}} = \frac{D \cdot L^2 \cdot (ax+b)^2}{V_{max} + L \cdot (ax+b)}$

The effect of photodegradation of machinery depends on the average turnover rate of the machinery before it is degraded via other means or diluted away by cell division. In steady state, the fraction of phototrophic protein that is functional (P_f) is related to protein turnover rate (R, in s^{-1}) and v_i by equation S13:

Equation S13: $R = R \cdot P_f + v_i \cdot P_f$

Rearranging this equation after substitution with Equation S12 results in Equation S14 for P_f:

Equation S14: $P_f = \frac{R}{R + v_i} = \frac{R}{R + \frac{D \cdot L^2 \cdot (ax+b)^2}{V_{max} + L \cdot (ax+b)}}$

This equation represents the factor by which previously calculated rates and efficiencies must be multiplied in order to determine the true rate of energy transduction, taking into account protein inactivation by light. Thus, we multiply equations S9 and S10 by equation S14 to obtain equations S15 and S16, which will be used for our final analysis:

Equation S15: $F_P = \frac{Y \cdot L \cdot V_{max} \cdot (ax+b)}{(k+x) \cdot (V_{max} + L \cdot (ax+b))} \cdot \frac{R}{R + \frac{D \cdot L^2 \cdot (ax+b)^2}{V_{max} + L \cdot (ax+b)}}$

Equation S16: $F_L = \frac{Y \cdot V_{max} \cdot (ax+b)}{(k+x) \cdot (V_{max} + L \cdot (ax+b))} \cdot \frac{R}{R + \frac{D \cdot L^2 \cdot (ax+b)^2}{V_{max} + L \cdot (ax+b)}}$

Numerical analysis

For purposes of numerical calculation of optimal architectures and performances, light intensities between a high of 4000 micromoles of photons per square meter per second (24.08 photons $Å^{-2}\ s^{-1}$), approximating the intensity of direct sunlight, and a low of $1 \cdot 10^{-2}$ micromoles of photons per square meter per second ($6.02 \cdot 10^{-5}$ photons $Å^{-2}\ s^{-1}$) were considered, with 1,000 light intensities distributed logarithmically across the range considered.

At every light intensity, the optimal antenna mass *x* must be determined for chlorophototrophic machinery and for retinalophototrophic machinery. As solving the optimum antenna mass *x* for maximizing F_P and F_L was analytically intractable, we numerically approximated it to the nearest 0.1 kDa at every tested light intensity, creating a table of optimal antenna masses x_{opt} for each light intensity for both sets of machinery.

All previously described variables were calculated at each light intensity for chlorophototrophs and retinalophototrophs using input variables described in Table S7, and the calculated optimal

antenna table. Values of F_P and F_L for the optimal system were recorded at all light intensities, as was the optimal antenna mass, and the ratio of F_p between chrlorophototrophs and retinalophototrophs. The light intensity, F_P, and F_L of the crossover point at which chlorophototrophy and retinalophototrophy were equivalent was also recorded. Variables are converted from light intensities in photons per second per square angstrom to intensities in micromoles of photons per square meter per second in order to make comparison to values in the literature easier.

Variable values used in calculation

Photodegradation and non-photodegradation protein turnover was considered to be the same for chlorophototrophs and retinalophototrophs for simplicity, and because the goal of this analysis is to determine which phototrophic system would be preferred in the same phototrophic ecological niche. The photodegradation rate constant D was taken to be $1.6 \cdot 10^{-6}$ $photon^{-1}$ from a Faizi et al. model of optimal phototrophic growth[21]. The non-photodegradation protein turnover rate R depends on the dilution timescale of protein in rapidly dividing cells, or the recycling of protein in non-dividing cells. It was taken to be 0.1 hr^{-1}, or 2.78·10-5 s^{-1}, for all analyses. This results in a half-life of protein machinery of approximately 6.93 hours, comparable to the protein dilution timescale of cyanobacteria undergoing exponential growth in bright light[21, 22].

Retinalophototrophy was represented by bacteriorhodopsin, with all numbers as previously described above (table S6, reproduced in table S7) except for the absorption cross section which was recalculated to take into account differing absorption across the visible spectrum. This was calculated by averaging the absorption spectrum of a rhodopsin [23] across the PAR (Photosynthetically Active Radiation) range of 400 to 700 nanometers, normalized to an

extinction coefficient ε of 62700 $M^{-1}cm^{-1}$ at 549 nm[24]. The absorption spectrum was only measured to 424 nm, and all values between this and 400 nm were represented as the same value as 424 nm. This averaged to an extinction coefficient εa across all PAR of 25667 which using Equation S17[25] is translated into an absorption cross section b of 0.982 $Å^2$.

Equation S17: $b = \varepsilon a \cdot \frac{2303}{6.02 \cdot 10^{23} M^{-1} \cdot 1cm}$

Chlorophototrophy was similarly represented by an anoxygenic proteobacterial type 2 RC as described above, since it was the chlorophototrophic system most easily decomposed into a discrete central engine and antenna. The anoxygenic RC engine requires an absorption cross-section b and mass k in isolation without any attached antenna complexes. Absorption cross section was approximated by multiplying the number of bound photopigments by their cross sections. The composition of the *Thermochromatium tepidum* reaction center was used to extrapolate the absorption cross section of a minimal chlorophototrophic reaction center. This contains four bacteriochlorophyll and two bacteriopheophytin molecules and one integral spirilloxanthin carotenoid[10, 26, 27]. Absorption spectra were obtained via personal communication with Dr. Canniffe of the University of Liverpool The spectrum of bacteriochlorophyll was normalized to an extinction coefficient of 92000 $M^{-1}cm^{-1}$ at 781 nm[28], that of bacteriopheophytin a to 45100 $M^{-1}cm^{-1}$ at 747 nm[29], and that of spirilloxanthin to 101400 $M^{-1}cm^{-1}$ at 525 nm[29]. All were averaged across the PAR range of 400 to 700 nm. Using equation S17, the absorption cross section of bacteriochlorophyll came to 0.476 $Å^2$, bacteriopheophytin came to 0.236 $Å^2$, and spirilloxanthin came to 1.390 $Å^2$. The spirilloxanthin carotenoid was considered to transfer 40% of its absorbed photons, as it has a role in quenching and a low quantum efficiency [30]. Thus, the total absorption cross section of the *T tepidum*

central reaction center comes to approximately 2.932 $Å^2$. Mass was approximated by subtracting the mass of the LH1 ring, leaving a central engine with a core homologous to those of other reaction centers with a mass of approximately 150 kDa.

Lastly, an absorption cross section per unit mass of antenna was required. The same value was used for both chlorophototrophic antennas, and hypothetical antennas connected to rhodopsins. This was taken to be approximately 0.163 $Å^2\ kDa^{-1}$. This is the value obtained by dividing the sum of the absorption cross section of all pigments in the LH2 antenna complex[11] (18 bacteriochlorophyll and 9 spirilloxanthin) by the mass of the LH2 antenna complex (130 kDa). The full absorption cross section for spirilloxanthin was used, as the quantum efficiency of photon absorption by antenna carotenoids in LH1 and LH2 can approach 100%[30]. All variables are recorded in Table S7.

Table S7: Variables for calculation of efficiency per unit light and efficiency per unit infrastructure of chlorophototrophic and retinalophototrophic machinery

	Bacteriorhodopsin	Anoxygenic RC
k (kDa)	26	150
b ($Å^2$)	0.982	2.392
Vmax (s^{-1})	100	150
Y (protons $cycle^{-1}$)	1	2
a ($Å^2$ kDa^{-1})	0.163	0.163
D ($photon^{-1}$)	$1.6 \cdot 10^{-6}$	$1.6 \cdot 10^{-6}$
R (s^{-1})	$2.78 \cdot 10^{-5}$	$2.78 \cdot 10^{-5}$

Results

Supplemental figure 2A, and 2C through 2F depicts the emergent trade-off between efficiency per unit protein and efficiency per unit incident light for chlorophototrophs and retinalophototrophs in the form of a plot of the optimal F_P versus F_t. Every separate point on the solid green and purple lines represents the efficiencies of a different optimal phototrophic system at a given light intensity. At all other light intensities they are strictly inferior in all respects to a better-optimized phototrophic system of the same type, except in the degenerate case of a system which is best with zero antenna at a range of light intensities, which occurs at the highest light

intensities for chlorophototrophy. The optimal systems together define a Pareto front, representing a trade-off between efficiency per unit protein infrastructure and efficiency per unit light resource. At high light levels (above ~185 micromoles of photons per square meter per square meter per second) retinalophototrophs dominate with high energy flux per unit protein, while at low light levels retinalophototrophs dominate with high efficiency per unit incident light.

Notably, as the equations for FP and F_L differ only by a factor of light intensity L, regardless of the system being used, Equation S18 holds:

Equation S18: $\frac{F_L}{F_P} = \frac{1}{L}$

This means that at a given light intensity, any phototrophic system regardless of its properties will lie somewhere on a line passing through the origin with a slope inversely proportional to the light intensity.

The curves describing the optimization of the two systems cross at a critical light intensity of 186 micromoles of photons per square meter per second, with retinalophototrophy producing both higher optimal F_P and F_L at higher light intensities but chlorophototrophy superior at lower light intensities. Again, as the equations for F_P and F_L are identical except for a factor of light intensity, at a given light intensity the advantage of a given phototrophic system is identical for both.

Supplemental figure 2b illustrates the optimal antenna mass for chlorophototrophs and retinalophototrophs at different light intensities. At the crossover point, the optimal chlorophototroph is calculated to have an antenna mass of 95.4 kDa and the optimal

retinalophototroph is calculated to have an antenna mass of 60.8 kDa. These values climb without bound as light level decreases to zero, but as light intensity increases they reach zero for chlorophototrophy by 1845 micromoles of photons per kilodalton per second, and decrease to only 2.1 kDa for retinalophototrophy at the maximum light intensity examined.

These values comport well with the observed makeup of real-world phototrophic machinery. Chlorophototrophs' antenna complexes range all the way in size up to massive crystalline chlorosomes which can be significant fractions of the size of a bacterium[31] and have even been observed on the ocean floor[32]. There is no known chlorophototrophic reaction center in nature that does not bear antenna complexes, with all type I reaction centers bearing "core" antennas which are part of the same polypeptide chain, and type II reaction centers either bearing a LH1 ring permanently associated with the complex in the case of anoxygenic reaction centers or a core antenna related to that of type I reaction centers but in a separate polypeptide in the case of photosystem II. The minimum antenna complex associated with a reaction center is approximately 130 kDa in the form of the sum of the core antennas of the dimeric heliobacteria reaction center[33] – remarkably close to the predicted value of the smallest antenna.

Real-world retinalophototrophic machinery has only ever been observed to contain single carotenoid molecules attached to the sides of xanthorhodopsin molecules as antennas[34], rather than any more elaborate antenna complexes. The calculated largest optimal antenna of the retinalophototrophic machinery closest to the crossover point is approximately the same size as the smallest known antenna complex – a single copy of the heliobacterial core antenna at 65 kDa. This would, however, only be useful at the very lowest light levels that retinalophototrophs

are superior at, possibly limiting the utility of tying these sorts of antenna complexes into this pathway.

Supplemental figure 3 illustrates the relative advantage of chlorophototrophs and retinalophototrophs at different light intensities. This was calculated by computing the ratio of F_P for the two systems at all light intensities. At low light intensities chlorophototrophy has nearly a 2-fold advantage in our model, while at high light intensities the advantage shifts to retinalophototrophy and increases to over 3-fold in unfiltered direct sunlight.

Importantly, the crossover point between the chlorophototroph and retinalophototrophic curve is dependent on the turnover rate R of the phototrophic machinery – as turnover rate decreases, there is more opportunity for photodegradation and small differences in photodegradation rate compound into larger differences in the functional fraction of machinery. This variable is highly dependent on metabolic state and growth rate, and so any one value is only representative of a small set of physiological conditions. We performed an analysis of the sensitivity of the modeled crossover light level to the base protein turnover rate R. See Supplemental figure 4 for a plot of crossover light intensity versus both protein turnover rate R, and the half-life of phototrophic protein machinery. Half-life was calculated using Equation S19.

Equation S19: $Half\ Life = \frac{\ln(2)}{R}$

At extremely fast physiologically unlikely turnover rates, the crossover point rises rapidly in light intensity, with the crossover point reaching 578 micromoles of photons per square meter per second at a R of 1 hr^{-1} and a half-life of 0.69 hours, faster than any known phototrophic doubling time. As turnover rates slow down the crossover point drops in light intensity, with it

reaching 47 micromoles of photons per square meter per second at a half-life/doubling time of 100 hours and as low as 17.7 micromoles of photos per square meter per second at an R of 0.001 hr^{-1} and a half-life of 693 hours. As turnover rate can depend on either protein recycling or dilution due to cell division, we should expect a crossover between chlorophototrophic and retinalophototrophic advantage at lower light levels when considering slow-growing metabolically quiescent cells as compared to fast-growing metabolically active cells, consistent with its observed role in preventing starvation[35]. While these crossover light levels vary over a factor of thirty as we allow the recycling and dilution rate R to vary 0.001 hr^{-1} to 1 hr^{-1}, they remain much dimmer than direct sunlight and the trade-off curves of F_L vs F_P retain a similar qualitative relationship – see supplemental figure 4 C through E.

In order to confirm the real-world ecological significance of the calculated critical light intensity, we analyzed the distribution of retinal and chlorophylls at depth in the ocean as previously described by Gómez-Consarnau et al[36]. Taking raw data from a transect of the Mediterranean Sea, we isolated every datapoint and examined the total flux of photosynthetically active radiation (PAR), the concentration of retinal pigment, and the total quantity of chlorophyll-a plus the concentration of bacteriochlorophyll. Unmeasurably low values were taken to be zero. We sorted these datapoints by PAR intensity, performed a rolling average of 10 datapoints to smooth noise, and normalized pigment concentrations to their average concentration across all datapoints to account for different average absolute concentrations of chlorophyll and retinal pigments. Supplemental figure 5 illustrates the resultant summary of relative concentration of chlorophototrophic and retinalophototrophic pigments at different PAR levels in a transect of the open ocean. The pattern is roughly consistent with the relative advantages of chlorophototrophy versus retinalophototrophy as calculated in our model – chlorophototrophic pigments are above

their average concentration at light intensities below our calculated crossover point, and retinalophototrophic pigments are above their average concentration at light intensities above our calculated crossover point, although the threshold is not sharp. This could be the result of the previously noted dependence of the favorability of phototrophic mode on the recycling rate of the machinery, and the presence of many different growth rate populations in the ocean. This may also be because the ocean is dynamic and mixed rather than perfectly stratified by light level, and because even as both chlorophototrophy and retinalophototrophy produce biological energy, they do have important physiological and ecological differences – for example retinalophototrophy cannot produce biomass no matter what light intensity it is exposed to, and requires no limiting iron in resource-poor environments. We thus observe qualitative evidence for the accuracy of our calculation of the ecological partitioning of phototrophic niche space between chlorophototrophs and retinalophototrophs.

Works Cited:

1. Oesterhelt, D. and W. Stoeckenius, *Rhodopsin-like protein from the purple membrane of Halobacterium halobium.* Nature new biology, 1971. **233**(39): p. 149-152.
2. Béja, O., et al., *Bacterial rhodopsin: evidence for a new type of phototrophy in the sea.* Science, 2000. **289**(5486): p. 1902-1906.
3. Cunningham, F.X., et al., *Stoichiometry of photosystem I, photosystem II, and phycobilisomes in the red alga Porphyridium cruentum as a function of growth irradiance.* Plant physiology, 1989. **91**(3): p. 1179-1187.
4. Umena, Y., et al., *Crystal structure of oxygen-evolving photosystem II at a resolution of 1.9 Å.* Nature, 2011. **473**(7345): p. 55-60.
5. Fromme, P., P. Jordan, and N. Krauß, *Structure of photosystem I.* Biochimica et Biophysica Acta (BBA)-Bioenergetics, 2001. **1507**(1-3): p. 5-31.
6. Zhang, J., et al., *Structure of phycobilisome from the red alga Griffithsia pacifica.* Nature, 2017. **551**(7678): p. 57-63.
7. Singharoy, A., et al., *Atoms to Phenotypes: Molecular Design Principles of Cellular Energy Metabolism.* Cell, 2019. **179**(5): p. 1098-1111. e23.
8. Muench, S.P., J. Trinick, and M.A. Harrison, *Structural divergence of the rotary ATPases.* Quarterly reviews of biophysics, 2011. **44**(3): p. 311-356.
9. Scheuring, S. and J.N. Sturgis, *Atomic force microscopy of the bacterial photosynthetic apparatus: plain pictures of an elaborate machinery.* Photosynthesis research, 2009. **102**(2-3): p. 197-211.
10. Niwa, S., et al., *Structure of the LH1–RC complex from Thermochromatium tepidum at 3.0 Å.* Nature, 2014. **508**(7495): p. 228-232.
11. Cherezov, V., et al., *Room to move: crystallizing membrane proteins in swollen lipidic mesophases.* Journal of molecular biology, 2006. **357**(5): p. 1605-1618.
12. Kolber, Z.S., et al., *Bacterial photosynthesis in surface waters of the open ocean.* Nature, 2000. **407**(6801): p. 177-179.
13. Lubner, C.E., et al., *Solar hydrogen-producing bionanodevice outperforms natural photosynthesis.* Proceedings of the National Academy of Sciences, 2011. **108**(52): p. 20988-20991.
14. Nawrocki, W., et al., *The mechanism of cyclic electron flow.* Biochimica et Biophysica Acta (BBA)-Bioenergetics, 2019.
15. Friedrich, T., et al., *Proteorhodopsin is a light-driven proton pump with variable vectoriality.* Journal of molecular biology, 2002. **321**(5): p. 821-838.
16. Lanyi, J.K., *Proton transfers in the bacteriorhodopsin photocycle.* Biochimica et Biophysica Acta (BBA)-Bioenergetics, 2006. **1757**(8): p. 1012-1018.
17. Walter, J.M., et al., *Light-powering Escherichia coli with proteorhodopsin.* Proceedings of the National Academy of Sciences, 2007. **104**(7): p. 2408-2412.
18. Kirchman, D.L. and T.E. Hanson, *Bioenergetics of photoheterotrophic bacteria in the oceans.* Environmental microbiology reports, 2013. **5**(2): p. 188-199.
19. Sener, M., et al., *Overall energy conversion efficiency of a photosynthetic vesicle.* elife, 2016. **5**: p. e09541.
20. Han, B.-P., *A mechanistic model of algal photoinhibition induced by photodamage to photosystem-II.* Journal of theoretical biology, 2002. **214**(4): p. 519-527.
21. Faizi, M., et al., *A model of optimal protein allocation during phototrophic growth.* Biosystems, 2018. **166**: p. 26-36.

22. Zavřel, T., et al., *Characterization of a model cyanobacterium Synechocystis sp. PCC 6803 autotrophic growth in a flat-panel photobioreactor.* Engineering in Life Sciences, 2015. **15**(1): p. 122-132.
23. Inoue, K., et al., *Red-shifting mutation of light-driven sodium-pump rhodopsin.* Nature communications, 2019. **10**(1): p. 1-11.
24. Rehorek, M. and M.P. Heyn, *Binding of all-trans-retinal to the purple membrane. Evidence for cooperativity and determination of the extinction coefficient.* Biochemistry, 1979. **18**(22): p. 4977-4983.
25. She, C., et al., *Low-threshold stimulated emission using colloidal quantum wells.* Nano letters, 2014. **14**(5): p. 2772-2777.
26. Yu, L.J., et al., *Structural Basis for the Unusual Qy Red-Shift and Enhanced Thermostability of the LH1 Complex from Thermochromatium tepidum.* Biochemistry, 2016. **55**(47): p. 6495-6504.
27. Noy, D., C.C. Moser, and P.L. Dutton, *Design and engineering of photosynthetic light-harvesting and electron transfer using length, time, and energy scales.* Biochim Biophys Acta, 2006. **1757**(2): p. 90-105.
28. Connolly, J.S., E.B. Samuel, and A.F. Janzen, *Effects of solvent on the fluorescence properties of bacteriochlorophyll a.* Photochemistry and photobiology, 1982. **36**(5): p. 565-574.
29. van der Rest, M. and G. Gingras, *The pigment complement of the photosynthetic reaction center isolated from Rhodospirillum rubrum.* Journal of Biological Chemistry, 1974. **249**(20): p. 6446-6453.
30. Noguchi, T., H. Hayashi, and M. Tasumi, *Factors controlling the efficiency of energy transfer from carotenoids to bacteriochlorophyll in purple photosynthetic bacteria.* Biochimica et Biophysica Acta (BBA)-Bioenergetics, 1990. **1017**(3): p. 280-290.
31. Kouyianou, K., et al., *The chlorosome of Chlorobaculum tepidum: size, mass and protein composition revealed by electron microscopy, dynamic light scattering and mass spectrometry-driven proteomics.* Proteomics, 2011. **11**(14): p. 2867-80.
32. Beatty, J.T., et al., *An obligately photosynthetic bacterial anaerobe from a deep-sea hydrothermal vent.* Proceedings of the National Academy of Sciences, 2005. **102**(26): p. 9306-9310.
33. Gisriel, C., et al., *Structure of a symmetric photosynthetic reaction center–photosystem.* Science, 2017. **357**(6355): p. 1021-1025.
34. Balashov, S.P., et al., *Xanthorhodopsin: a proton pump with a light-harvesting carotenoid antenna.* Science, 2005. **309**(5743): p. 2061-4.
35. Gómez-Consarnau, L., et al., *Proteorhodopsin Phototrophy Promotes Survival of Marine Bacteria during Starvation.* PLOS Biology, 2010. **8**(4): p. e1000358.
36. Gómez-Consarnau, L., et al., *Microbial rhodopsins are major contributors to the solar energy captured in the sea.* Science advances, 2019. **5**(8): p. eaaw8855.
37. Raven, J.A., *Contributions of anoxygenic and oxygenic phototrophy and chemolithotrophy to carbon and oxygen fluxes in aquatic environments.* Aquatic Microbial Ecology, 2009. **56**(2-3): p. 177-192.
38. Canfield, D.E., M.T. Rosing, and C. Bjerrum, *Early anaerobic metabolisms.* Philosophical Transactions of the Royal Society B: Biological Sciences, 2006. **361**(1474): p. 1819-1836.
39. Sleep, N.H. and D.K. Bird, *Niches of the pre-photosynthetic biosphere and geologic preservation of Earth's earliest ecology.* Geobiology, 2007. **5**(2): p. 101-117.
40. Kimura, Y., et al., *Surface of bacteriorhodopsin revealed by high-resolution electron crystallography.* Nature, 1997. **389**(6647): p. 206-211.

459 41. Tomasello, G., I. Armenia, and G. Molla, *The Protein Imager: a full-featured online molecular*
460 *viewer interface with server-side HQ-rendering capabilities.* Bioinformatics, 2020. **36**(9): p. 2909-
461 2911.

462

Supplemental Figures

Supplemental Figure 1: Phototrophic vs Chemolithoautotrophic Primary Production

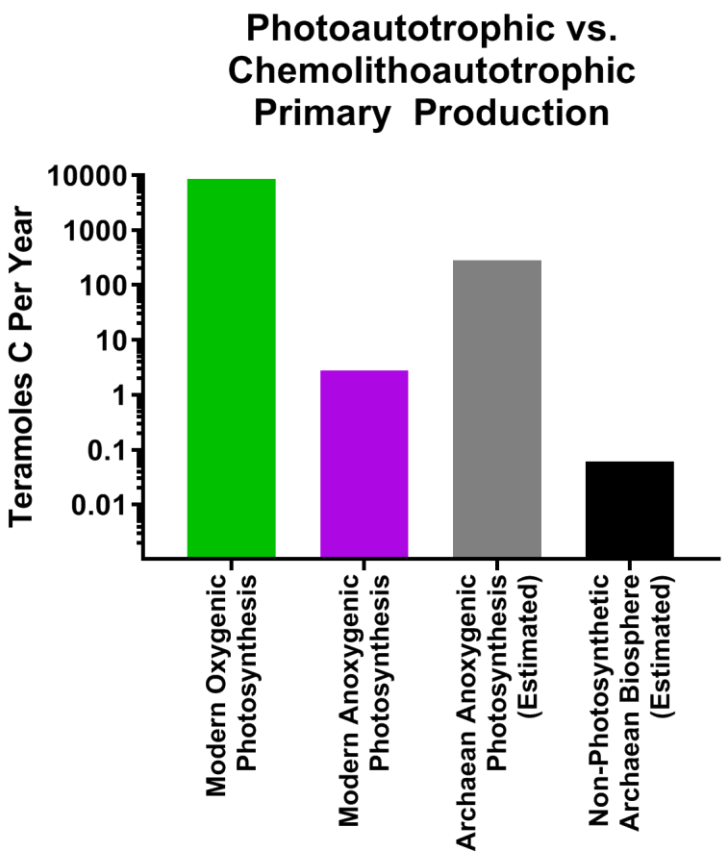

Legend: Comparison between carbon flux through biospheres driven by photosynthesis and chemolithoautotrophy. Modern oxygenic photosynthesis drives carbon fixation of nearly 9,000 teramoles per year[1]. While modern anoxygenic photosynthesis represents at most ~2.7 teramoles per year [2], estimates of anoxygenic photosynthesis in the Archaean are ~280 teramoles per year [3]. Estimates of possible carbon flux through a pre-photosynthetic, entirely chemolithotrophic biosphere driven by Archaean geochemical fluxes alone are circa 0.06 teramoles per year [4].

Supplemental Figure 2: Model Results for Optimal Chlorophototrophic and Retinalophototrophic Machinery at Different Light Levels

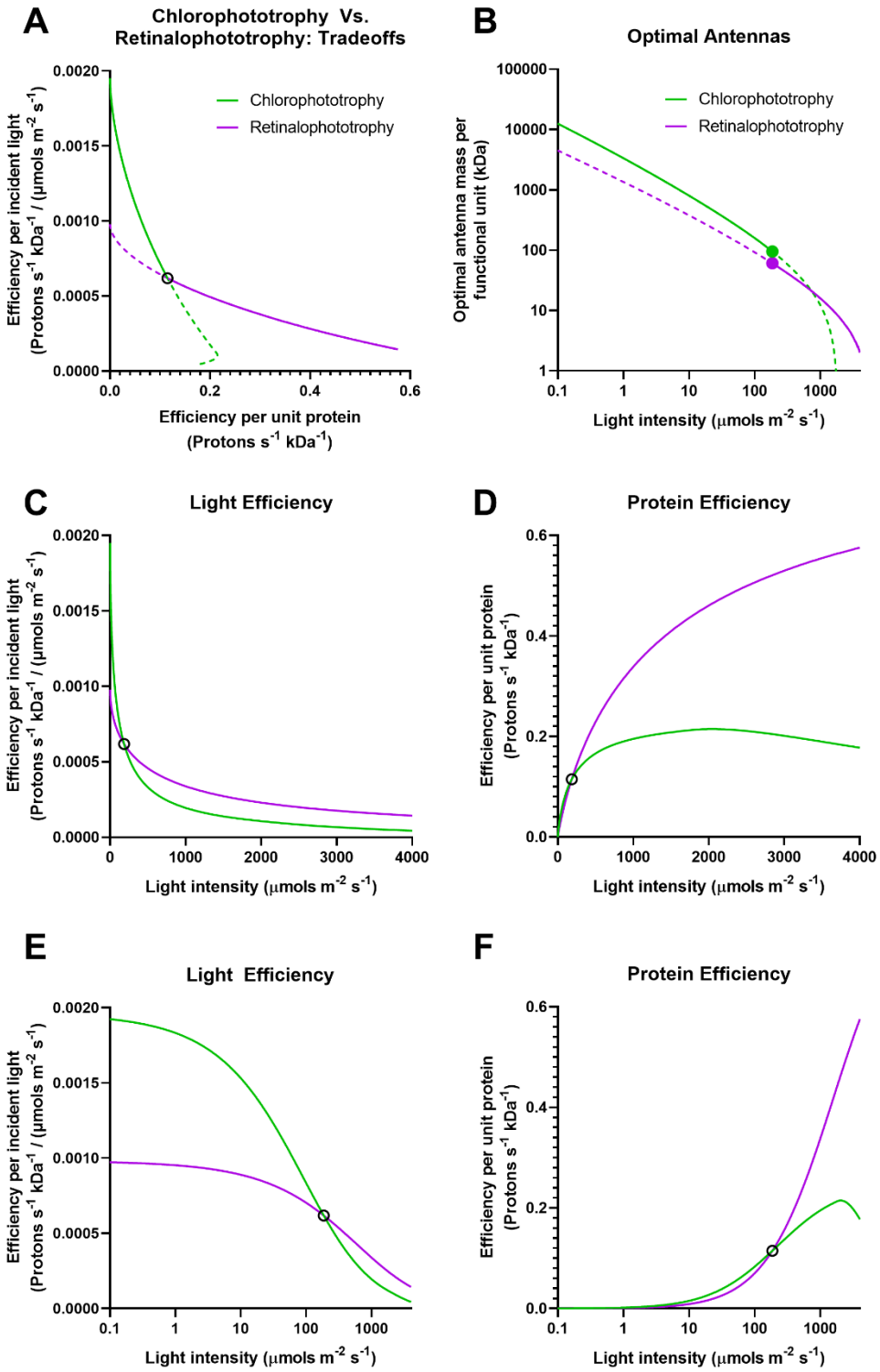

Legend: A) Modeled trade-off between efficiency per unit protein and efficiency per unit light for chlorophototrophy and retinalophototrophy. The optimal system at a given light intensity is pictured as a solid line, with the sub-optimal system at a given light intensity pictured as a dotted line. The crossover point is indicated with an open circle. B) The optimal antenna mass modeled for chlorophototrophs and retinalophototrophs graphed across different light intensities, pictured as in the previous panel. The optimal antenna for both systems rises to arbitrarily large masses at low light levels, before falling to zero at less than the maximum modeled light intensity for chlorophototrophs and near zero at the maximum modeled light intensity for retinalophototrophs. The crossover point at which both systems are modeled as equivalent is indicated via solid circles. C) Efficiency per unit light versus light intensity, with light intensity on a linear scale. Crossover point indicated. D) Energy flux per unit protein, with light intensity on a linear scale. Crossover point is indicated. E) Efficiency per unit light versus light intensity, with light intensity on a logarithmic scale. F) Energy flux per unit protein versus light intensity, with light intensity on a logarithmic scale.

Supplemental Figure 3: Relative Advantages of Chlorophototrophs and Retinalophototrophs at Different Light Intensities

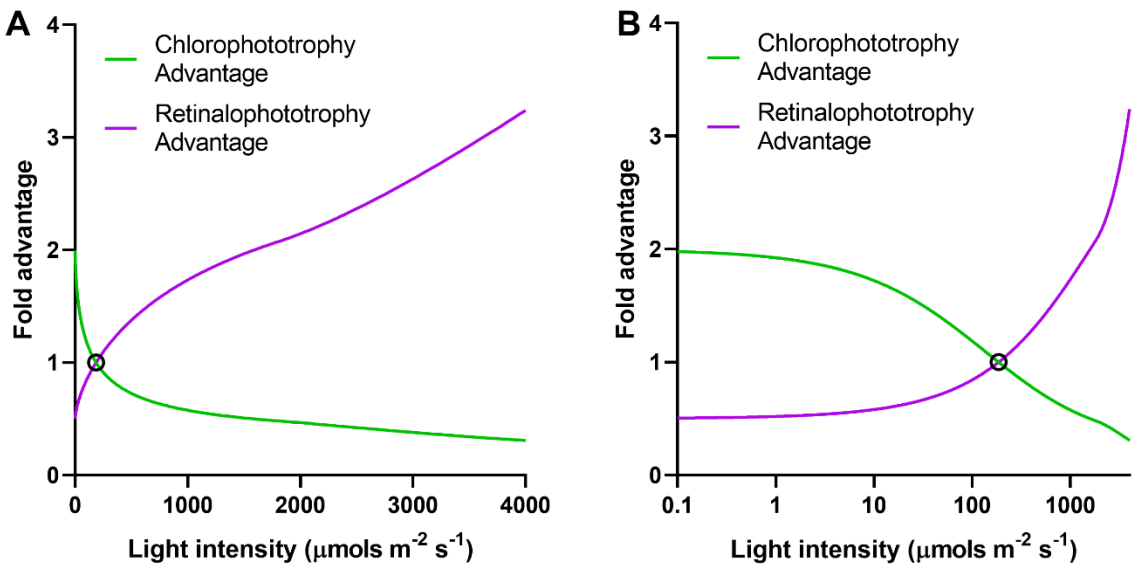

Legend: A) The fold advantage of the optimal calculated chlorophototrophic system and retinalophototrophic system at different light intensities. Both systems are evenly matched in terms of energy flux per unit protein, or efficiency per unit light, at a light intensity of 186 micromoles of photons per square meter per second. At low light intensity chlorophototrophs approach a nearly 2-fold advantage, while at high light levels the advantage of retinalophototrophs exceeds 3-fold. B) The same data, on a logarithmic light scale to enhance legibility.

Supplemental Figure 4: Sensitivity of Crossover Value to Degradation Rate Constant

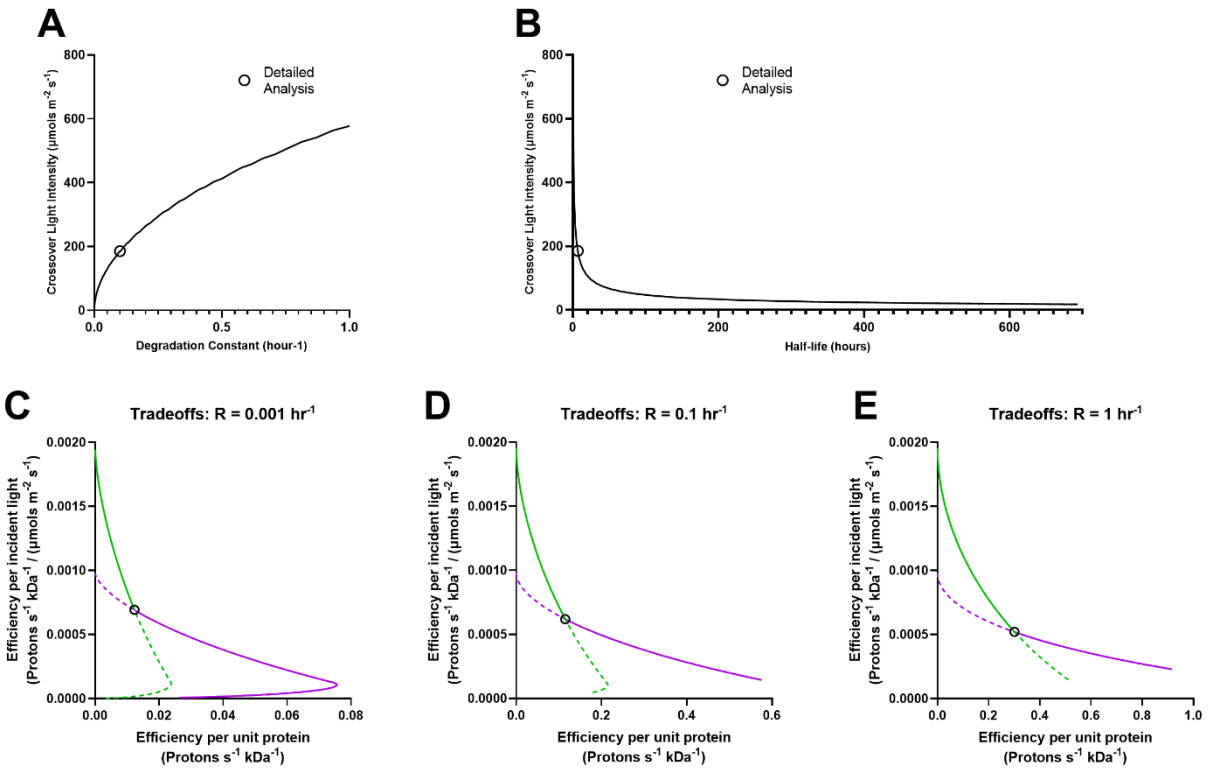

Legend: A) Sensitivity of the modeled crossover point of chlorophototrophy and retinalophototrophy to the degradation rate constant R. Open circle indicates the value used for detailed analysis in this publication. At a degradation constant of 0.001 hr^{-1} (half-life of 693 hours) a crossover point between chlorophototrophy and retinalophototrophy occurs at 17.7 µmols $m^{-2}s^{-1}$, at 0.1 hr^{-1} (half-life of 6.9 hours) it occurs at 185.6 µmols $m^{-2}s^{-1}$, and at 1 hr^{-1} (half-life of 0.69 hours) it occurs at 577.7 µmols $m^{-2}s^{-1}$. B) Sensitivity of the modeled crossover point to the non-photodegradation half-life of phototrophic machinery. Open circle indicates the value used for detailed analysis in this publication. C) Tradeoff of efficiency per unit protein versus efficiency per incident light with recycling/dilution rate of 0.001 hr^{-1}. D) Tradeoff of efficiency per unit protein versus efficiency per incident light with recycling/dilution rate of 0.1 hr^{-1}. E) Tradeoff of efficiency per unit protein versus efficiency per incident light with recycling/dilution rate of 1 hr^{-1}. Tradeoffs remain similar in form.

Supplemental Figure 5: Comparison of Calculated Properties of Chlorophototrophs and Retinalophototrophs, and Their Actual Distribution (Gómez-Consarnau et al.)

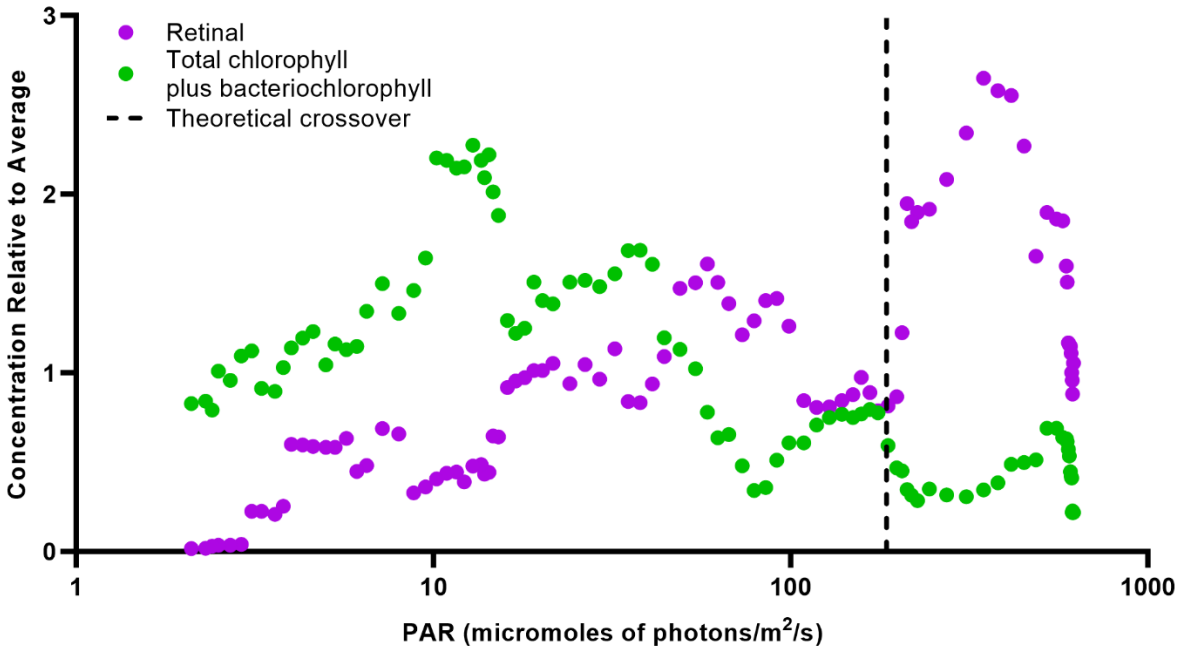

Legend: Smoothed data from Gómez-Consarnau et al.[5] on the distribution of chlorophototrophic and retinalophototrophic pigments in the water column. All values are normalized to the average concentration of pigment across the whole dataset. Dotted line indicates the modeled theoretical crossover point at which chlorophototrophy and retinalophototrophy are equivalent. The highest retinal pigment concentrations are observed above the modeled crossover point, and the highest chlorophototrophic pigment levels are observed below the crossover point.

Works Cited:

1. Field, C.B., et al., *Primary production of the biosphere: integrating terrestrial and oceanic components.* science, 1998. **281**(5374): p. 237-240.
2. Raven, J.A., *Contributions of anoxygenic and oxygenic phototrophy and chemolithotrophy to carbon and oxygen fluxes in aquatic environments.* Aquatic Microbial Ecology, 2009. **56**(2-3): p. 177-192.
3. Canfield, D.E., M.T. Rosing, and C. Bjerrum, *Early anaerobic metabolisms.* Philosophical Transactions of the Royal Society B: Biological Sciences, 2006. **361**(1474): p. 1819-1836.
4. Sleep, N.H. and D.K. Bird, *Niches of the pre-photosynthetic biosphere and geologic preservation of Earth's earliest ecology.* Geobiology, 2007. **5**(2): p. 101-117.
5. Gómez-Consarnau, L., et al., *Microbial rhodopsins are major contributors to the solar energy captured in the sea.* Science advances, 2019. **5**(8): p. eaaw8855.